DEPARTMENT OF TRANSPORTATION

Construction & Early Performance of Rapid Strength Cement Concrete Mixture in MnROAD Test Cell 2437

Bernard Igbafen Izevbekhai, Principal Investigator
Office of Materials & Road Research
Minnesota Department of Transportation

August 2025

Final Report NRRA202601

NRRA National Road Research Alliance

To get this document in an alternative format or language, please call 651-366-4720 (711 or 1-800-627-3529 for MN Relay). You can also email your request to ADArequest.dot@state.mn.us. Please make your request at least two weeks before you need the document.

Technical Report Documentation Page

1. Report No.	2.	3. Recipients Accession No.
NRRA202601		

4. Title and Subtitle	5. Report Date
Construction & Early Performance of Rapid Strength Cement Concrete Mixture in MnROAD Test Cell 2437	December 2025
	6.
Authors:	8. Performing Organization Report No.
Bernard Igbafen Izevbekhai MnDOT Research Operations Engineer Ceren Aydin MnDOT Geomechanics Research Engineer	
9. Performing Organization Name and Address	10. Project/Task/Work Unit No.
Minnesota Department of Transportation Office of Materials & Road Research 1400 Gervais Avenue Maplewood MN 55119	11. Contract (C) or Grant (G) No.
12. Sponsoring Organization Name and Address	13. Type of Report and Period Covered
Minnesota Department of Transportation Office of Research & Innovation 395 John Ireland Boulevard, MS 330 St. Paul, Minnesota 55155-1899	NRRA Final Report 2024-25
	14. Sponsoring Agency Code

15. Supplementary Notes

http://mdl.mndot.gov/

16. Abstract (Limit: 250 words)

This initiative constructed and studied a rapid strength gaining concrete mixture placed in MnROAD Test Cell 2437. The innovative concrete made from a belitic calcium sulfoaluminate (BCSA) cement was placed in a 36 ft by 12 ft test section on November 22, 2024, when the ambient temperature was approximately 35°F. The test cell was instrumented with vibrating wire strain gauges, thermistors, and maturity sensors to monitor strength development and performance. Initial laboratory results demonstrated high early compressive strength exceeding control mixtures. However, flexural strengths initially exceeded control cell values but was followed by an unexpected decline thus prompting petrographic and chemical analyses to further investigate internal structural integrity and hydration completeness.

Petrographic analysis revealed some microcracking, typical of accelerated strength gain but with no sign of frost damage in spite of the low temperatures that proceeded the paving. It also revealed induced micro-cracking dispersed within the matrix and filled with ettringite. The material also passed the durability ASTM C666 test and was found to be constructible in spite of some anomalous rheological thixotropic tendency it exhibited in transforming from a very mobile and workable mix quickly to a stiff mix within the period of placement and finishing. That feature was associated with early strength gain.

17. Document Analysis/Descriptors	18. Availability Statement
Thixotropic, MnROAD, BCSA	No restrictions. Document available from: National Technical Information Services, Alexandria, Virginia 22312

19. Security Class (this report)	20. Security Class (this page)	21. No. of Pages	22. Price
Unclassified	Unclassified	24	

Construction & Early Performance of Rapid Strength Cement Concrete Mixture in MnROAD Test Cell 2437

Final Report

Prepared by:

Bernard Igbafen Izevbekhai P.E., Ph.D.
MnDOT Office of Materials & Road Research

Ceren Aydin Ph.D.
MnDOT Office of Materials & Road Research

December 2025

Published by:

Minnesota Department of Transportation
Office of Research & Innovation
395 John Ireland Boulevard, MS 330
St. Paul, Minnesota 55155-1899

Acknowledgements

Authors are indebted to MnROAD Operations for their effort in instrumentation and placement of this short test cell. They also acknowledge Maria Masten and Rob Golish of the MnDOT Concrete Engineering Unit as well as Tom Burnham who was the Acting MnDOT Research Manager and Ben Worel, the MnROAD Research Operations Engineer and Executive Director of National Road Research Alliance (NRRA), during the conceptualization and placement of the test cell. The abovementioned and Eddie Johnson of the MnDOT Office of Materials and Road Research who constituted the technical advisory panel are acknowledged accordingly. Authors are grateful to Michael Vrtis, Assistant MnROAD Operations Engineer, and Jacob Calvert, MnROAD Monitoring and Testing Engineer, for facilitating construction testing and early data collection. The prep work and shouldering was performed by MnROAD's Jesse Shank and cold weather saw cutting was performed by MnROAD's Troy Huebner.

Names of Collaborators mentioned here are deemed pertinent to the report and are acknowledged

- Concrete Paving Association of Minnesota (CPAM) supplied ¾ inch dowels and provided drone flights and footage. (The ¾ in dowels were examined in a separate report)
- CTS Cement Manufacturing, Garden Grove CA commercialize a belitic calcium sulfoaluminate cement that they provided for the experiment.
- SJB Concrete St Paul MN provided the on-site volumetric mixer.
- North Country Concrete East Bethel MN placed the concrete.
- American Engineering Testing Inc St. Paul MN obtained samples on site and conducted rheological , mechanical strength and transport properties testing as retained by MnDOT.

Table of Contents

List of Tables

List of Figures

Executive Summary

This initiative constructed a 36-ft by 12-ft test section in the MnROAD low volume loop on November 22, 2024, when the ambient temperature was 35 degrees Fahrenheit. This dimension was cut out of the existing cell 37 up to the top of the base layer. MnROAD Operations compacted and refinished the base layer and provided and installed two concrete maturity sensors as well as 2 sets of vibrating wire strain gauges and thermistors.

The initiative investigates the field characteristics of concrete made utilizing a fast setting, rapid hardening cement. Accelerating strength gain is an important property desirable in concrete. Such a mixture was placed in MnROAD test cell 2437 on the November 22, 2024, using a roller screed. A volumetric mobile mixer was provided by a local concrete contractor.

In Chapter 1, a general introduction is provided. In Chapter 2, the Mix design and experimental design are discussed. In Chapter 3, the instrumentation and construction process are accentuated. In Chapter 4, the results of rheological and mechanical strength as well as transport properties are discussed. The material appeared to have attained very high compressive strength and high early flexural strength, but the latter reduced with time prompting petrographic analysis. Chapter 5 is dedicated to petrographic analysis of a core from the test cell as well as some X-ray diffraction of a sample obtained from the core.

The report concludes that the pavement material exhibited resiliency in facilitating paving at low temperature (35 Deg F) without negative consequences. Additionally, the pavement overcame freeze thaw conditions and a core taken from the pavement after 3 months passed the durability test.

Chapter 1: Introduction

1.1 Background

High early strength concrete is important in cold weather conditions (1) and in situations such as busy roadways where rapid reopening to traffic is required. A rapid strength Belitic Calcium Sulfoaluminate Cement (BCSA) concrete (2) (3) was placed in a 36-ft by 12-ft test cell at the MnROAD low volume road in November 2024. introduces lesser carbon footprint than Ordinary Portland cement.

1.2 MnROAD Test Cell 2437

A test cell (Cell 2437) with a concrete composed of rapid strength gaining cement was constructed at the MnROAD low-volume test track to evaluate its field performance under traffic and environmental factors. The initiative received a product research request from the manufacturers who commercialize a BCSA cement. A local concrete contractor provided a volumetric concrete mobile mixer on site. This report primarily studies the characteristics of a rapid strength gaining concrete (1), (2), (3) as a sustainable material. It consists in performing some of the rheological, mechanical, and transport property tests on samples obtained during construction, and from the instrumentation placed in the test cell. These include transverse and longitudinal vibrating wire strain gauges for top and bottom and concrete maturity sensors set to provide 56-day maturity data (4) & (5). It summarizes petrographic and x ray diffraction test results from analysis performed by a Local testing company (6) & (7).

Small diameter (¾-inch diameter dowels) were placed in the interior joints of the test cell to ascertain their suitability. That aspect is covered in another report.

1.3 Research Goals

This study documents construction and concomitant activities of the short test cell. It also analyzes preliminary results from early performance tests. While early performance is useful, continued monitoring of the cell is needed for full evaluation of the test cell. This research evaluates the product for suitability in paving.

1.4 Chapter Summary

This chapter introduces a belitic sulfoaluminate cement concrete as the material placed in cell 2437 at MnROAD. The next chapter discusses the experimental design and testing scheme.

Chapter 2: Experimental Design

2.1 Background

The previous chapter only introduced the rapid strength concrete without proprietary details. This chapter lays out a field-testing scheme for the concrete test cell (Tables 2.1 to 2.3).

2.1.1 Rheological, mechanical strength, transport properties and miscellaneous tests for cell 2437

Table 2.1 Rheological Properties for Cell 2437 Concrete

Test Method	Test Name	Sampling Frequency
C231/T152	Air Content	2 per cell during placement
C138	Unit Weight	2 per cell during placement
T119	Slump	2 per cell during placement
C1064	Temperature	2 per cell during placement

Table 2.2 Mechanical strength, transport properties and miscellaneous tests for cell 2437

Test Method	Test Name	Sampling Frequency
C39 - Compressive Strength- Laboratory Curing	Compressive Strength	4” x 8” cylinders during placement (1 set of 3) For 4-hours Test
		4” x 8” cylinders during placement (1 set of 3) For I day test
		4” x 8” cylinders during placement (1 set of 3) 3 days
		4” x 8” cylinders during placement (1 set of 3) for 7 days
		4” x 8” cylinders during placement (1 set of 3) for 28 days
C78 - Flexural Strength	Flexural Strength	6” x 6” x 20” beams during placement (set of 2) for 4 hour test
		6” x 6” x 20” beams during placement (set of 2) for 1 day test
		6” x 6” x 20” beams during placement (set of 2) for 3 day test
		6” x 6” x 20” beams during placement (set of 2) for 7 day test
		6” x 6” x 20” beams during placement (set of 2) For 28 day test
C1074/(MnDOT) Maturity		For 1, 3, 4, 7, 28 day tests
T358 (Transport) Surface Resistivity	1, 3, 7, 14, 28, days	Testing performed on 4x8 compressive strength specimens For 1, 3, 4, 7, 28 day tests

Table 2.3 Durability

Test Method	Test Name	Sampling Frequency
C666, Method A	Freeze-Thaw	1 set of 3
ASTM C157 Shrinkage	Drying Shrinkage (35, 56 days)	1 set of 3

2.2 Testing Notes

Due to the unique properties of the rapid hardening cement, manufacturers proactively conveyed the recommendation to modify test procedures for some properties of the concrete. Manufacturers recommended air curing and no moist curing for the concrete and recommended keeping the shrinkage and freeze-thaw specimens in air and not to moist cure either the shrinkage or freeze thaw specimens. As in the experimental design, the resistivity test scheme utilized compression test samples for the resistivity testing before being subjected to their corresponding tests. Tests for resistivity, were done on the compressive strength specimens. Consequently, a resistivity test was done on each specimen at each age. Specimens were kept in the curing room at 100% humidity until the time of testing per manufacturer recommendations.

The following variable was noted: “

[If the resistivity testing is done on a dry specimen, the results will be difficult to compare to any controls we have from other paving this year. The resistivity value is sensitive to conditioning. So, comparing a moist control to a dry rapid set will be an “apples to oranges” comparison] (Email correspondence with the manufacturer during construction)

2.2.1 Other Special Requirements

2.2.1.1 ASTM C157:

[Do not put the bars in a water tank. If you put RS specimens in water for 7 days, you will not capture any shrinkage afterward, and that is not actually how it really works in the field. What I am recommending is “against” the material because I am saying to take 24hr readings and then keep them air-drying for all the other measurements to be consistent with previous testing.] (Email correspondence with the manufacturer during construction)

2.2.1.2 ASTM C666:

[The specs do not require a specific time of saturation before testing. 14 days is standard in many labs, but the body of evidence supports a lot of shorter times (1 or 2 days of saturation). Modification recommended a saturation of 14 days as long as the specimens are air-cured first for 42 days. The reasoning was based on the fact that the concrete matrix develops and

"matures" differently from Portland cement mixes whereas all these tests were developed for Portland cement]. (Email correspondence with the manufacturer during construction)

2.2.1.3 Surface Resistivity AASHTO T358:

[Curing regime for these specimens is typically in water while testing is usually at 28 days, but we require specimens to be air-cured for those 28 days with testing at 1 day, 3 days, 7 days, and 28 days]. (Email correspondence with the manufacturer during construction)

2.3 Miscellaneous Items

Considering the very low temperature during paving, MnROAD Research personnel made provisions for thick insulating blankets to minimize the risk of frost. It also called for deadweights on the blankets to forestall wind effects and minimal removal during joint sawing and restoration of the cover thereafter.

2.4 Chapter Summary

In this chapter a testing and research plan was accentuated. The next chapter discusses the actual construction and associated activities.

Chapter 3: Instrumentation and Construction

3.1 Background

This initiative constructed a short test cell in the low-volume road of the MnROAD research facility. The previous chapter discussed standard testing and proposed tests as well as modifications to some standard tests. This chapter discusses the test site, actual pavement placement, finishing and curing.

3.2 MnROAD Research Facility

The MnROAD pavement research facility is operated by the Minnesota Department of Transportation (MnDOT). Constructed between 1990 and 1993 and opened to traffic in 1994, MnROAD is located on westbound I-94, northwest of the Twin Cities. The Mainline (3.5 miles of interstate westbound 94) and 2.5 miles of the low volume road (LVR) and the old westbound tracks make up the MnROAD facility, although other minor tracks including the stockpile area and the access road leading to the weather station contain some test cells. During periodic surface non-sensor measurements at MnROAD, live traffic is diverted to the old west-bound track. This 3.5-mile track also has test sections but not for accelerated loading scenarios.

MnROAD features dedicated pavement test cells equipped with sensors that monitor performance and assess the impact of traffic loads and environmental factors such as temperature fluctuations and drainage. In addition to these sensors, various tests, including the International Roughness Index (IRI), Falling Weight Deflectometer (FWD), On Board Sound Intensity OBSI, and Circular Track Meter (CTM), are conducted on the cells to evaluate different aspects of pavement designs and surface characteristics throughout their service life. The test cells in the Mainline are exposed to actual traffic conditions, while those in the LVR are subject to controlled traffic loading. The LVR is loaded by a dedicated truck with a gross vehicle weight (GVW) of 40 US tons, impacting only the inner lane, while the outer lane is affected solely by environmental loading.

Over the past thirty years, MnROAD has undergone many reconstruction phases to establish new test sections or replace expired sections. This test track is renowned for the plethora of variform designs and materials that characterize a wide range of pavement test cells (numbering up to 60 cells) where each cell is at least 76 m (250 ft) long and two 12-ft-wide lanes. The various designs facilitate extensive studies, as strain, moisture, temperature, and state (freeze thaw indication) are constantly and directly loading the database. This data is easily retrieved and can be analyzed to deduce trends in response of the pavements to traffic and environmental loads.

Certain performance measurements are not adapted to sensor installation and automatic data collection. These are measured directly when traffic is diverted from the test cells at Interstate 94 westbound (the Mainline) or when the 80 daily laps of the 80 kips 5-axle semitrailer on the low volume loop is interrupted to facilitate the falling weight deflectometer measurement for layer moduli and load transfer efficiency, friction, ride, and noise. Performance data is fed into the data base and can be

retrieved with a simple query. The test cell is located on the inside lane of the north side of the low volume loop.

3.3 Removals and Base

The slabs removed were not isolated for forensic evaluation but were discarded. Preliminary compaction was done until the instrumentation was anchored to the base, before a final finish was enhanced. Direct stormwater was not prevented from reaching the base between exposure and paving; however, outlets were provided at the shoulder to drain out excess stormwater that would otherwise have ponded the base. The original base material was a priori an overconsolidated MnDOT Class 5 aggregate base material. An excerpt of the preceding cell 37 between neighboring cells is shown in Figure 3.1.

3.4 Instrumentation and Paving

Figure 3.1 shows the test cell 2437 location. Figure 3.2 shows panels A, B and C along with the instrumentation.

	Cell 36	Cell 37	Cell 2437	Cell 37	Cell 138	Cell 238
	Original Concrete	Original Concrete 2007 Grind Strips	B-CSA Cement Concrete	Original Concrete 2007 Grind Strips	Low Cementitious Concrete	Lower Cementitious Concrete
	6" PCC 15'LX12'W Panels 1" Dowel Transverse Tining	6" PCC 12'LX12'W Panels 1" Dowel Transverse Tining	6" B-CSA 12'LX12'W Panels 3/4" Dowel Longitudinal Broom	6" PCC 12'LX12'W Panels 1" Dowel Transverse Tining	8" PCC 15'LX12'W Panels 1" Dowel Transverse Tining 500lb/yd^3 Cementitious	8" PCC 15'LX12'W Panels 1" Dowel Transverse Tining 470lb/yd^3 Cementitious
	5" Class 5	5" Class 5	5" Class 5	5" Class 5	5" Class 5	5" Class 5
	Sand	Sand	Sand	Sand	Sand	Sand
	Clay Subgrade	Clay Subgrade	Clay Subgrade	Clay Subgrade	Clay Subgrade	Clay Subgrade
Commissioned	Jul-93	Jul-93	Nov-24	Jul-93	Jul-17	Jul-17
Cell Length (ft)	480	504	36	504	240.5	270
Transition (ft)	127	0	0	0	42	19.5

Figure 3.1 Excerpt of MnROAD Test Cell Maps 2024 updated to show cell 2437 surrounded by cell 37 and neighboring cells

Figure 3.1 shows the test cell 2437 location. Figure 3.2 shows panels A, B and C along with the instrumentation.

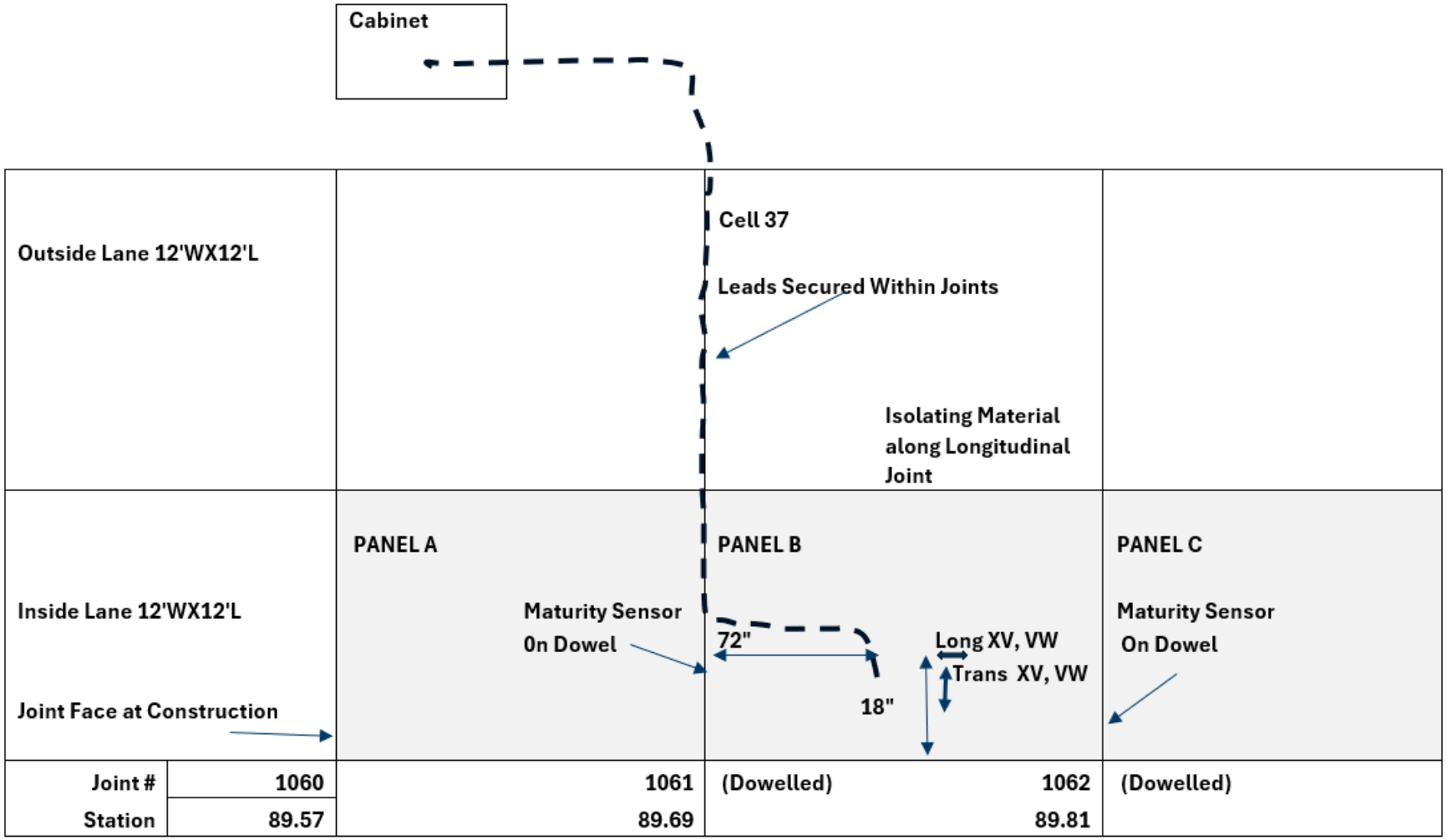

Figure 3.2 Instrumentation and location record

Figures 3.3 and 3.4 shows the maturity sensor installation on the dowel bar. They consist of a Body and cable sensor so that 2 sets of readings are provided by each sensor. While the body is installed approximately 2 inches below the concrete surface flexibility to capture maturity at an additional depth location of interest is provided by placement of the cable end at the depth of interest

Figure 3.3 Typical Maturity Sensor Installed

Figure 3.4 Typical instrumentation location for maturity sensor

Table 3.1 and Figure 3.2 show the location data for vibrating wire strain gauge with thermistor and maturity sensors. In total, four vibrating wire strain gauge and thermistor and two maturity sensors.

Table 3.1 Instrumentation and location data

Vibrating Wire Strain Gauge and Thermistor							
Model	**Seq**	**Orientation**	**Sensor Name**	**Approx. STA**	**Offset (ft)**	**Depth (in)**	**Material**
VW	1	Longitudinal	2437VW01	89+75.85	10.5	1	Concrete
VW	2	Longitudinal	2437VW02	89+75.86	10.5	5	Concrete
VW	3	Transverse	2437VW03	89+75.87	10.75	1	Concrete
VW	4	Transverse	2437VW04	89+75.88	10.75	5	Concrete

Maturity	
Maturity Datalogger Body and Cord	Joint 1061
Maturity Datalogger Body and Cord	Joint 1062

Figure 3.5 shows transverse and longitudinal vibrating wire strain gauges installed and anchored to plastic supports and connected through leads to the cabinet (not shown) near the test cell.

Figure 3.5 Vibrating wire strain gauges

The preexisting pavement was cut out by MnROAD forces on November 10, 2024, using power concrete cutters that ensured a smooth vertical edge around the entire perimeter of the 36-ft by 12-ft section (Figure 3.6).

Figure 3.6 Aerial view of the low volume road and inset: Cell 2437 in perspective

Placement began at 9:00am on 11/22/2024. The air temperature during paving was 35 degrees Fahrenheit. MnDOT used an existing contract with a local concrete paving contractor. A local testing company was retained to do plastic, rheological, mechanical, and transport properties testing. Samples were obtained for strength, shrinkage, and freeze-thaw testing at the local independent testing company. Figures 3.7 to Figure 3.10 show the paving process.

Figure 3.7 Picture accentuating sensor location and paving progression

Figure 3.8 A panoramic view looking Northwest

Figure 3.9 Aerial view of the pavement placement process progressing from NW to SE

Figure 3.10 Aerial view (looking east) of the pavement placement process progressing from NW to SE showing the cables extending through the outside lane towards the cabinets. (Cabinets are not shown)

Figure 3.11 shows how cold weather protection was accomplished after broom texturing.

Figure 3.11 Insulative blankets were placed on the test cels after paving , finishing, texturing and applying curing compound (Alpha Methyl Styrene).

The material was characterized by initial high mobility and workability, but during placement it rapidly stiffened, thus exhibiting anomalous thixotropic behavior. Evident anomalous thixotropy of this material necessitated accelerated finishing since it provided only a short window between placement and setting. The surface was successfully finished and broom textured. Poly-alpha-methyl styrene curing compound was applied uniformly over the surface before it was covered with a double layer insulating blanket (Figure 3.11), held down by dead weights outside of the paved slabs. Due to the characteristic rapidity of strength gain exhibited by the material, early joint establishment by saw cutting was feasible and MnROAD forces commenced sawing within 3 hours of paving. Transverse joints were sawn to a 2-inch depth. This sawing process did not generate sliver spalls as would be typical of early sawing when the concrete has not gained sufficient strength.

3.5 Chapter Summary

This chapter has described the test site and test cell and introduced certain test modifications suggested by the product manufacturers. The next chapter discusses the various rheological, mechanical, transport and durability test results.

Chapter 4: Initial Laboratory Test Results and Pavement Performance Data

4.1 Background

The previous chapter enunciated construction layout, removals and placement. This chapter discusses the initial test results. In this chapter, the rheological mechanical strength and transport properties data were provided form testing conducted by American Engineering Testing who were contractually retained for the purpose.

4.2 Data Tables

Table 4.1 and Table 4.2 show four hour and one day test results of compressive strength and flexural strength. Data was provided by the independent testing company.

Table 4.1 Four Hour Test Result

Compression (psi)				Flexural (psi)		
1	2	3	Average	1	2	Average
3,378	**3,913**	**4,151**	3,814	410	320	**365**

Table 4.2 One day test result

C39 1 day: Compressive Strength (psi)				C78 1-day Flexural Strength (psi)		
1	2	3	Average	1	2	Average
5,140	4,840	4,890	4,960	525	455	490

Table 4.3 and Table 4.4 show rheological properties and ASTM C-157 expansion test results respectively.

Table 4.3 Rheological properties

ID	Test Type	Date Paved	Time of Day	Lab Id	Slump (in)	Air Content (%)	Unit Weight lb/ft^3	Concrete Temp (°F)
2437-I-2024	FP	11/22/2024	9:08 AM	AET	4.00	8.40	138.0	63
2437-I-2024	FP	11/22/2024	9:40 AM	AET	7.00	5.80	141.2	64

Table 4.4 ASTM C-157 Expansion Test Result

ID	Test Type	Cast Date	Initial Reading	Date Tested	Age	Exposure Time, Days	Exposure Type	Length Change %	Average Length Change %
2437-I-2024C157A	C157	11/22/2024	11/23/2024	11/23/2024	1	0	demolding	0.000	
2437-I-2024C157B	C157	11/22/2024	11/23/2024	11/23/2024	1	0	demolding	0.000	
2437-I-2024C157C	C157	11/22/2024	11/23/2024	11/23/2024	1	0	demolding	0.000	0.000
2437-I-2024C157A	C157	11/22/2024	11/23/2024	12/20/2024	28	0	soak	-0.002	
2437-I-2024C157B	C157	11/22/2024	11/23/2024	12/20/2024	28	0	soak	-0.002	
2437-I-2024C157C	C157	11/22/2024	11/23/2024	12/20/2024	28	0	soak	-0.003	-0.002
2437-I-2024C157A	C157	11/22/2024	11/23/2024	12/24/2024	32	4	dry	-0.002	
2437-I-2024C157B	C157	11/22/2024	11/23/2024	12/24/2024	32	4	dry	-0.002	
2437-I-2024C157C	C157	11/22/2024	11/23/2024	12/24/2024	32	4	dry	-0.003	-0.002
2437-I-2024C157A	C157	11/22/2024	11/23/2024	12/27/2024	35	7	dry	-0.006	
2437-I-2024C157B	C157	11/22/2024	11/23/2024	12/27/2024	35	7	dry	-0.006	
2437-I-2024C157C	C157	11/22/2024	11/23/2024	12/27/2024	35	7	dry	-0.007	-0.006
2437-I-2024C157A	C157	11/22/2024	11/23/2024	1/3/2025	42	14	dry	-0.013	
2437-I-2024C157B	C157	11/22/2024	11/23/2024	1/3/2025	42	14	dry	-0.013	
2437-I-2024C157C	C157	11/22/2024	11/23/2024	1/3/2025	42	14	dry	-0.014	-0.013
2437-I-2024C157A	C157	11/22/2024	11/23/2024	1/17/2025	56	28	dry	-0.009	
2437-I-2024C157B	C157	11/22/2024	11/23/2024	1/17/2025	56	28	dry	-0.009	
2437-I-2024C157C	C157	11/22/2024	11/23/2024	1/17/2025	56	28	dry	-0.010	-0.009

Figure 4.1 and Figure 4.2 show flexural and compressive strength of concrete compared to a control cell, respectively. 5 Table 4.5 shows Compressive strength, and flexural strength respectively.

Table 4.5 Compressive (a) and flexural (b) strength measurements

a) Compressive

Test Age	Fracture Type	Max Load	Strength_PSI	Diameter_in.	Length_in.	Area	Weight_lbs
4 hours	5	42,616	**3,378**	4.008	8.044	12.62	8.28
4 hours	2	48,639	**3,913**	3.978	8.087	12.43	8.11
4 hours	2	51,797	**4,151**	3.986	8.065	12.48	8.29
1 day	2	64,055	**5,141**	3.983	8.100	12.46	8.18
1 day	2	60,916	**4,840**	4.003	8.071	12.59	8.11

Test Age	Fracture Type	Max Load	Strength_PSI	Diameter_in.	Length_in.	Area	Weight_lbs
1 day	2	61,562	**4,887**	4.005	8.065	12.60	8.20
3 days	2	65,173	**5,207**	3.992	8.053	12.52	8.24
3 days	3	65,560	**5,238**	3.992	8.054	12.52	8.23
3 days	2	68,673	**5,498**	3.988	8.016	12.49	8.18
7 days	2	73,022	**5,814**	3.999	8.029	12.56	8.21
7 days	2	70,262	**5,617**	3.991	8.077	12.51	8.20
7 days	2	74,897	**5,975**	3.995	8.041	12.53	8.26
28 days	2	77,552	**6,181**	3.997	8.054	12.55	8.32
28 days	2	90,002	**7,205**	3.988	8.056	12.49	8.44
28 days	2	90,127	**7,194**	3.994	8.086	12.53	8.43

b) Flexural

MNROAD ID	SAMPLE ID	DATE PAVED	DATE TESTED	TEST AGE DAYS	FLEX STRENGTH PSI
2437-I-2024C78	A	11/22/2024	11/22/2024	0.17	410
2437-I-2024C78	B	11/22/2024	11/22/2024	0.17	320
2437-I-2024C78	A	11/22/2024	11/23/2024	1	525
2437-I-2024C78	B	11/22/2024	11/23/2024	1	455
2437-I-2024C78	A	11/22/2024	11/25/2024	3	630
2437-I-2024C78	B	11/22/2024	11/25/2024	3	520
2437-I-2024C78	A	11/22/2024	11/29/2024	7	535
2437-I-2024C78	B	11/22/2024	11/29/2024	7	490
2437-I-2024C78	A	11/22/2024	12/20/2024	28	485
2437-I-2024C78	B	11/22/2024	12/20/2024	28	450

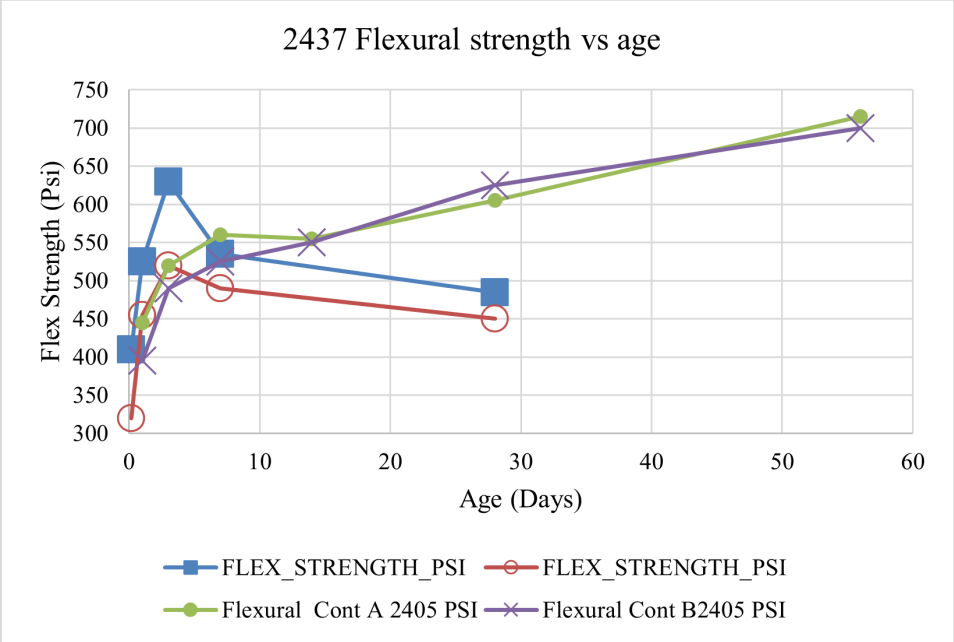

Figure 4.1 Flexural Strength Compared to a Control Cell.

In Figure 4.1, strength reduction portrayed is not normative but the cause here is unknown. Microcracking and handling are possible causes, but these are not established causes in this experiment.

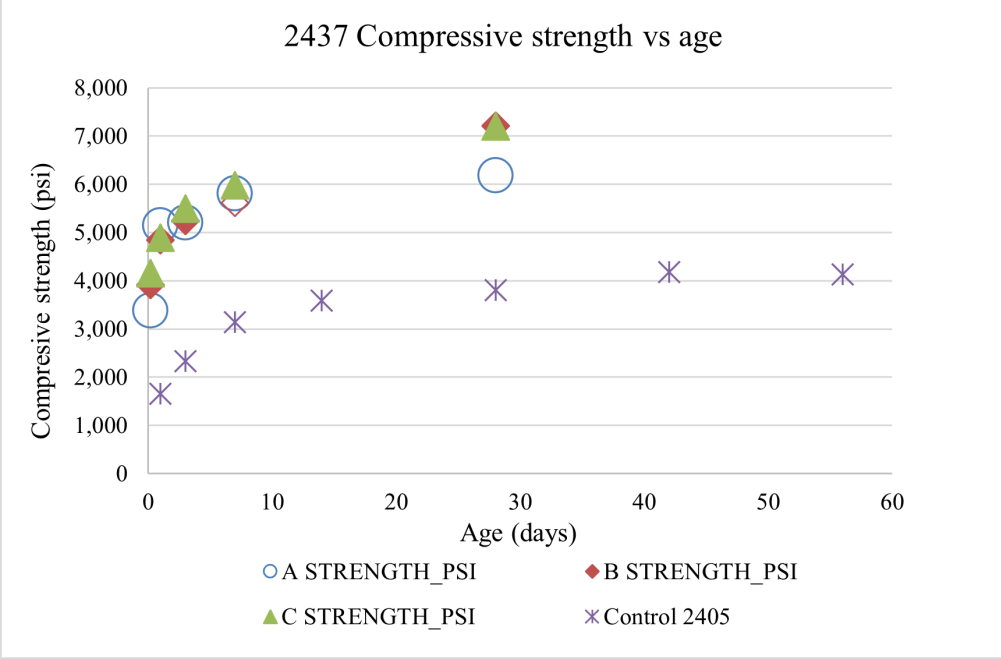

Figure 4.2 Compressive strength compared to a control cell.

In Figures 4.1 and 4.2, flexural and compressive strengths respectively are compared to the observed trend with respect to age observed in the control cell 2405 in the Mainline 2024 construction. Figure 4.3 and Figure 4.4 show the expansion test results with respect to exposure time and with respect to age, respectively.

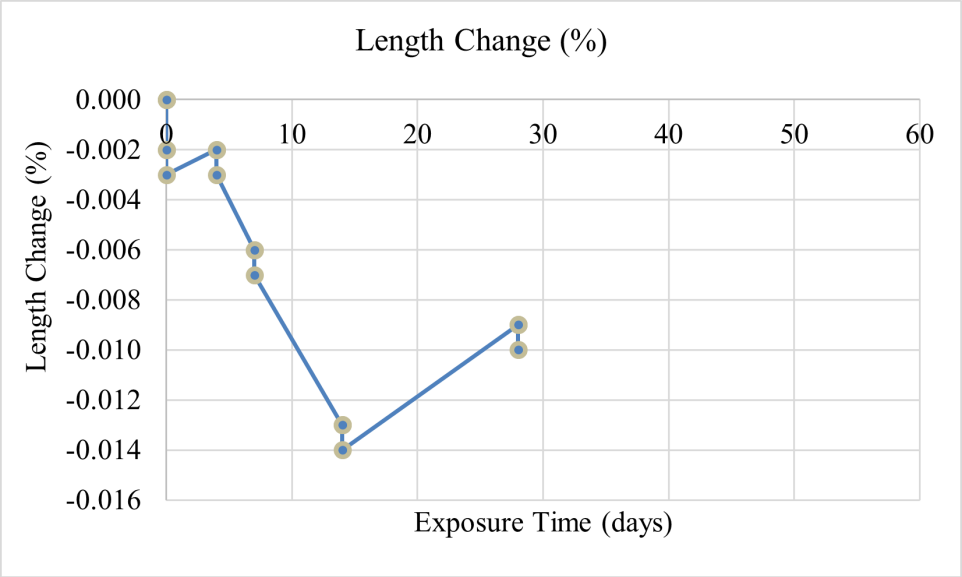

Figure 4.3 Expansion test results, expansion vs exposed time

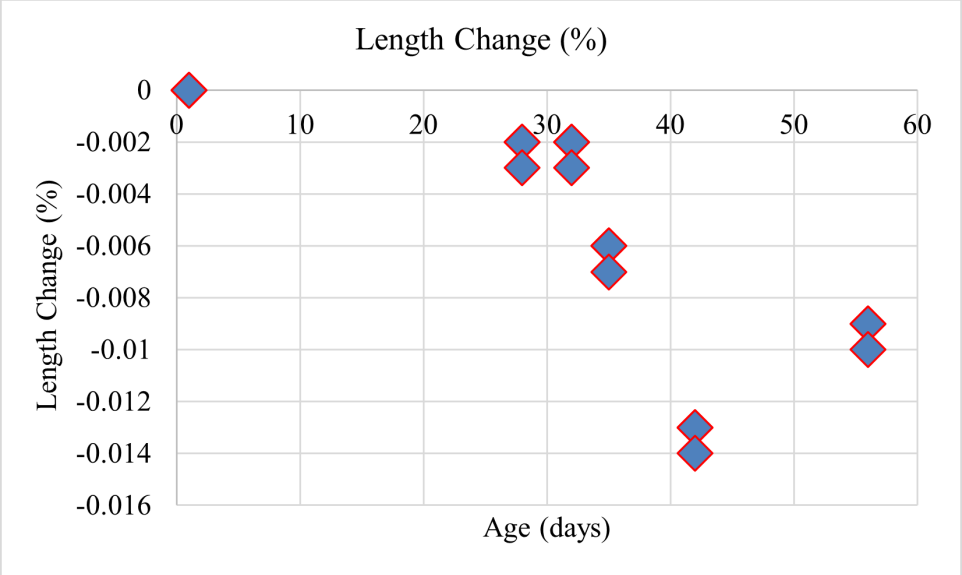

Figure 4.4 Expansion vs age

Table 4.6 shows surface resistivity test results.

Table 4.6 Surface Resistivity

Age	Resistivity Corrected for Limewater, KΩ-cm
4 Hours	25.01
4 Hours	25.84
4 Hours	25.63
3 days	26.98
3 days	34.28
3 days	35.48
7 days	26.61
7 days	29.12
7 days	32.93
28 days	33.51
28 days	38.62
28 days	38.7

Figure 4.5 and Figure 4.6 show resistivity trend and thermistor data, respectively.

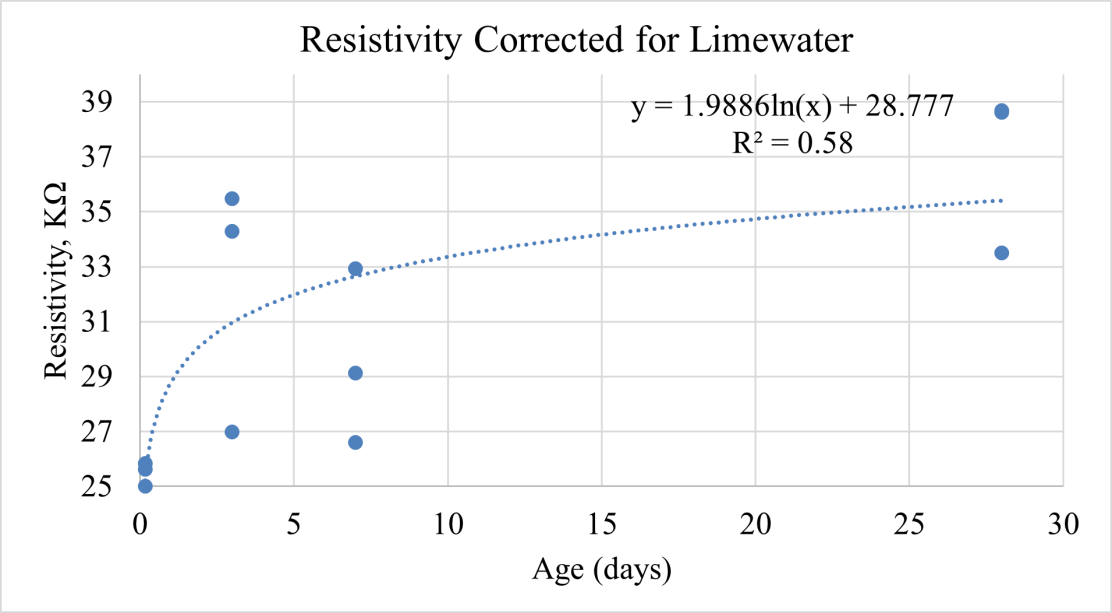

Figure 4.5 Resistivity Trends

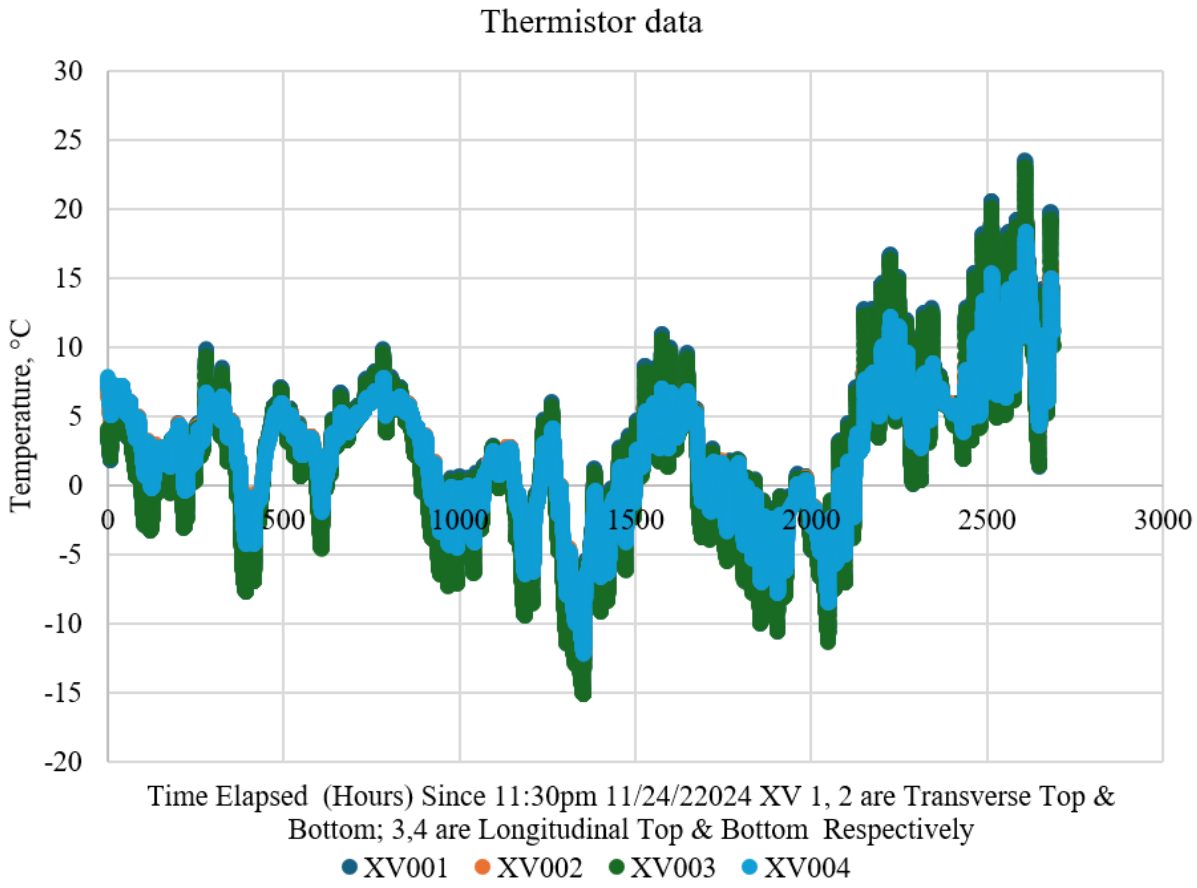

Figure 4.6 Thermistor data showing subzero encounters few days after paving

The top thermistors 1 (XV001) and 3 (XV003) in Figure 4.6 seem to show the highest amplitude in their time series. This phenomenon is a thermal factor and not a material factor. The data shows daily swings as well as many other wavelengths. Figure 4.7 shows the vibrating wire strain data.

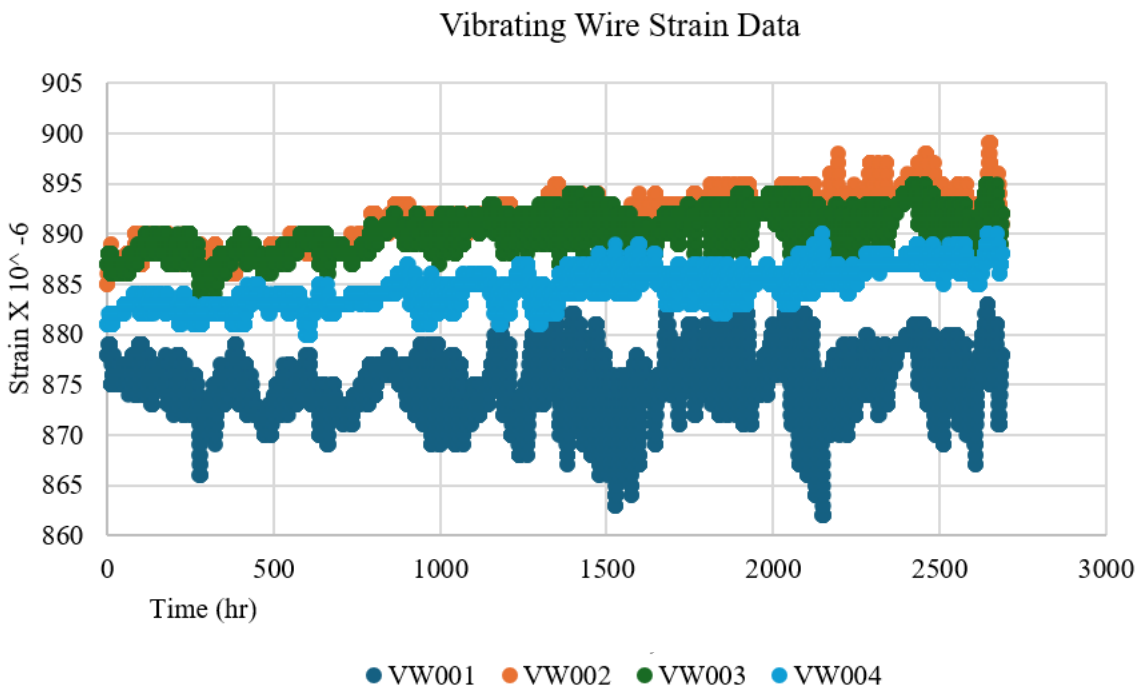

Figure 4.7 Vibrating wire strain gauge data

Strain in Figure 4.7 showed temperature fluctuations in the top and bottom sensors Longitudinal sensors are sensor 1 (top) and sensor 2 (bottom). Transverse sensors are sensor 3 (top) and sensor 4 (bottom)._ This phenomenon may also be environmentally induced and not material related. The pair of transverse top and longitudinal bottom sensors show the overall highest strain. The dispersion 861 to 899 micro-strain is infinitesimal and does not show widespread core versus exterior temperature variability to be of statistical significance.

4.3 Concrete Maturity

Table 4.7 shows maturity data for sensor 1.

Table 4.7 Excerpt (Microcosm) of Maturity Data (at inception) 2437- Sensor 1

Data			Analysis								Data	
					SI UNIT		Using area		SUM (TA-Tdatum) dt			
Date & Time	Cable Temp (DegF)	Body Temp (Deg F)	Diff (Deg F)	Age (HR)	T Cable	T Body	M Cable	M Body	SIGMA cable	Sigma Body	Comp (psi)	Flex (psi)
2024-11-22 11:19:37	72.34	71.69	0.65	0.25	22.4	22.1	5.6	5.5	5.6	5.5		
2024-11-22 11:34:37	71.58	73.08	1.5	0.5	22.0	22.8	11.0	11.4	16.6	16.9		
2024-11-22 11:49:37	71.24	71.96	0.72	0.75	21.8	22.2	16.4	16.7	32.9	33.6		
2024-11-22 12:04:37	71.06	71.44	0.38	1	21.7	21.9	21.7	21.9	54.6	55.5		
2024-11-22 12:19:37	70.99	71.2	0.21	1.25	21.7	21.8	27.1	27.2	81.7	82.7		
2024-11-22 12:34:37	71.02	71.15	0.13	1.5	21.7	21.8	32.5	32.6	114.2	115.3		
2024-11-22 12:49:37	59.2	43	16.2	1.75	15.1	6.1	26.4	10.7	140.7	126.0		
2024-11-22 13:04:37	60.78	59.54	1.24	2	16.0	15.3	32.0	30.6	172.7	156.6		
2024-11-22 13:19:37	61.39	61.88	0.49	2.25	16.3	16.6	36.7	37.4	209.4	194.0		
2024-11-22 13:34:37	62.02	62.4	0.38	2.5	16.7	16.9	41.7	42.2	251.1	236.2		
2024-11-22 13:49:37	62.96	63.63	0.67	2.75	17.2	17.6	47.3	48.3	298.4	284.5		
2024-11-22 14:04:37	64.54	65.88	1.34	3	18.1	18.8	54.2	56.5	352.6	341.0		
2024-11-22 14:19:37	67.42	69.19	1.77	3.25	19.7	20.7	64.0	67.1	416.6	408.1		
2024-11-22 14:34:37	78.6	80.58	1.98	3.5	25.9	27.0	90.6	94.5	507.2	502.6		
2024-11-22 14:49:37	84.42	89.06	4.64	3.75	29.1	31.7	109.2	118.9	616.4	621.5		
2024-11-22 15:04:37	87.21	92.37	5.16	4	30.7	33.5	122.7	134.2	739.1	755.6	3814	365

Table 4.8 shows the maturity analyses for Sensor 1 compressive and flexural strength. Figure 4.7 shows the vibrating wire strain data

Table 4.8 Maturity Analysis For Compressive Strength

Comp (Psi) M (Deg C-Hr)	M (Deg C-Hr)	Model	SQ Residual
0	0		0.0
3814	755	3844.7	941.1
4955.981	23160.77	4864.2	8419.7
5315	129179.4	5376.1	3730.3

Sum of squared residuals = 13091.2

Maturity data for Sensor 1 cable and sensor 1 body was similar to maturity data for Sensor 2 Body and Sensor 2 cable (Data was paltry).

The maturity equations (4) & (5) minimizing residuals:

Compressive: S= a + b log M

Solutions

a=1871.2 b=685.7

Model: F_c = 1871 + 685.7 Log M where Fc is compressive strength (psi), and M is Maturity in DegC-Hr

Table 4.9 Maturity Analysis for Flexural Strength

Flex (Psi) M (Deg C-Hr)	M (Deg C-Hr)	Model	SQ Residual
0	0		0.0
365	755	361.8	10.1
490	23160.77	499.5	90.7
575	129179.4	568.7	40.2

SumSqRes = 141.0

Flexural (psi) F_t= a + b log M

Solutions

a=95.3 and b=b=92.6

Model: F_t = 95.3 + 92.6 Log M where F_t is Flexural strength (psi), and M is Maturity in DegC-Hr

The two maturity data loggers provided data up to 56 days. Table 4.8 shows the analysis that was conducted on data from Sensor 1 for compressive strength and Table 4.9 shows the same for flexural strength. The analysis shown in Table 4.8 was performed on the Sensor Body data (each sensor provides data at "body" and at "end of cable") (Figure 3.3 and 3.4). The results obtained showed that sensor 1 body data was very similar to the other 3 data sets, including body and cable from Sensor 2. Just before the seventh day, the recorded temperatures fell below freezing point. The hydration of cement and gain in strength of the concrete is dependent on both curing time and temperature. Thus, the strength of the concrete may be expressed as some function of time and temperature (8). This information is used to determine the strength of concrete without conducting physical tests after training the function with corresponding strengths from compressive or flexural strength tests. The time-temperature function commonly used is the maturity concept proposed by Nurse-Saul (ASTM C1074) (Equation 4.1):

$$M\ (°C \times hours) = \sum [(T - T_0)\ \Delta t] \qquad 4.1$$

Where M is the maturity in °C-hours (M is also termed the time-temperature factor (TTF)), Δt is the time interval in hours (or days), T is the average concrete temperature during the time interval Δt, and T_0 is the datum temperature at which concrete ceases to gain strength with time. The value of T_0 = (0 °C) is most commonly used. As a result, Equation 4.1 becomes Equation 4.2:

$$M\ (°C \times hours) = \sum [(T)\ \Delta t] \qquad 4.2$$

Consequently, the concrete maturity prediction model was developed with the early strength and maturity data at 4-hours, 1-day and 3-days. Using the model (Equation 4.3),

$$S = a + b \log M \qquad 4.3$$

where S is compressive (or tensile) strength (psi), and M is maturity (°C-Hr).

Analysis minimizing least squared residuals resulted in Equation 4.4,

$$\text{Model: } Fc = 1871 + 685.7 \log M \qquad 4.4$$

where Fc is compressive strength (psi), and M is Maturity in °C-Hr.

Furthermore, it resulted in model, Equation 4.5,

$$Ft = 95.3 + 92.6 \log M \qquad 4.5$$

where Ft is tensile strength (psi), and M is Maturity in °C-Hr.

As a caveat, the above analysis was limited to early strength values because the pavement froze on the 6th day. The curve should have been influenced by the 7-day and 28-day strengths if tenable maturity values were available otherwise.

4.4 Durability Test

Table 4.10 shows Relative Dynamic Modulus (RDM) / Durability Factor (DF), mass change and Length change as results obtained from durability test ASTM C 666, Method A. The sample passed this durability test. This is significant especially considering the adverse factors such as freezing conditions. This result also buttresses the fact that there was no observable freeze thaw damage despite early exposure to freezing temperatures. Figures 4.8 to 4.10 plotted these results respectively.

Table 4.10 Durability Test Results Showing Relative Dynamic Modulus, Mass Change and Length Change

Test	Cycles	RDM 101	RDM 102	RDM 103	Average
Relative Dynamic Modulus	0	100	100	100	100
	36	98	100	100	99
	72	98	98	100	99
	108	98	98	98	98
	144	100	100	100	100
	180	98	100	98	99
	216	100	100	100	100
	252	100	100	100	100
	288	102	100	100	101
	300	102	98	100	100
		102	98	100	100
Mass Change	0	0	0	0	0.00
	36	-0.03	0.02	0.03	0.01
	72	-0.05	-0.06	0.03	-0.03
	108	0.01	-0.1	0.05	-0.01
	144	-0.03	-0.11	-0.01	-0.05
	180	-0.07	-0.2	-0.14	-0.14
	216	-0.19	-0.33	-0.21	-0.24
	252	-0.14	-0.43	-0.18	-0.25
	288	-0.13	-0.57	-0.22	-0.31
	300	-0.17	-0.64	-0.22	-0.34

Test	Cycles	RDM 101	RDM 102	RDM 103	Average
Length Change %	0	0	0	0	0.00
	36	0.01	0.01	0.01	0.01
	72	0.02	0.02	0.02	0.02
	108	0.01	0.01	0.01	0.01
	144	0.01	0.02	0.01	0.01
	180	0.02	0.03	0.02	0.02
	216	0.01	0.03	0.02	0.02
	252	0.02	0.03	0.02	0.02
	288	0.01	0.02	0.01	0.01
	300	0.01	0.02	0.01	0.01

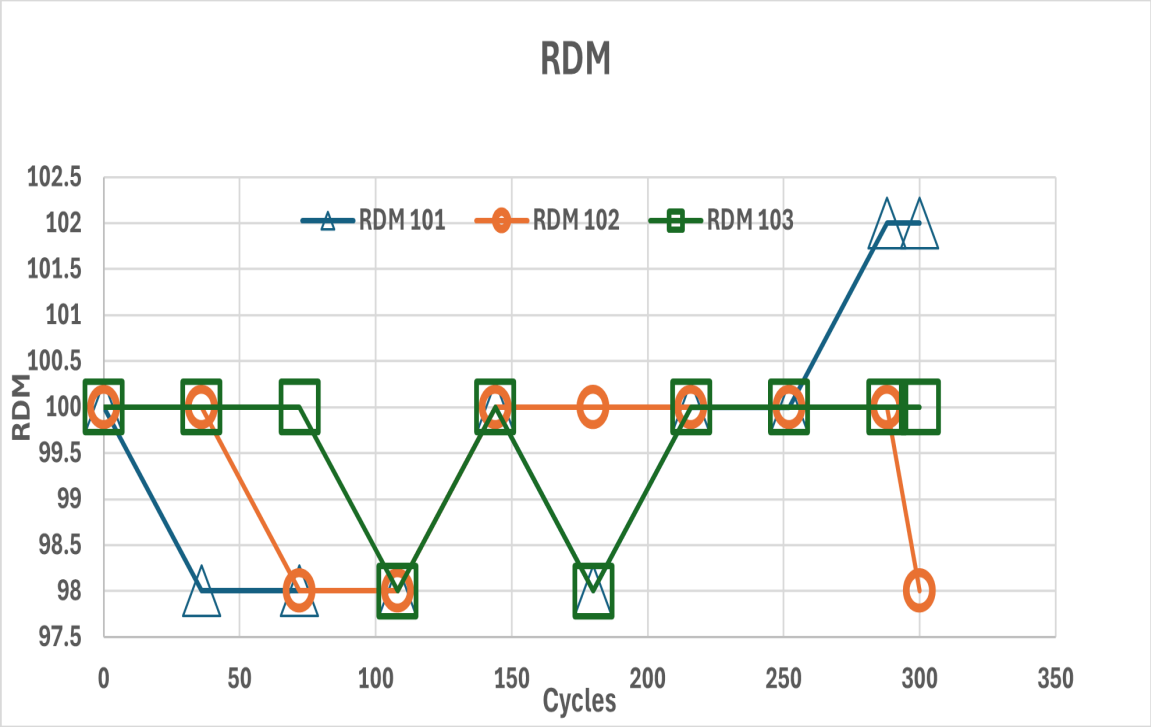

Figure 4.8 Relative Dynamic Modulus

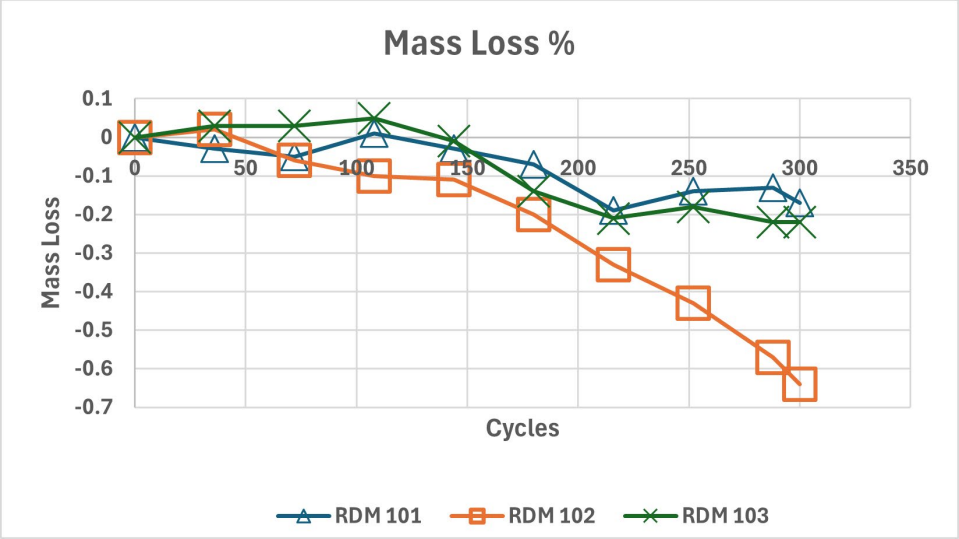

Figure 4.9 Mass Change

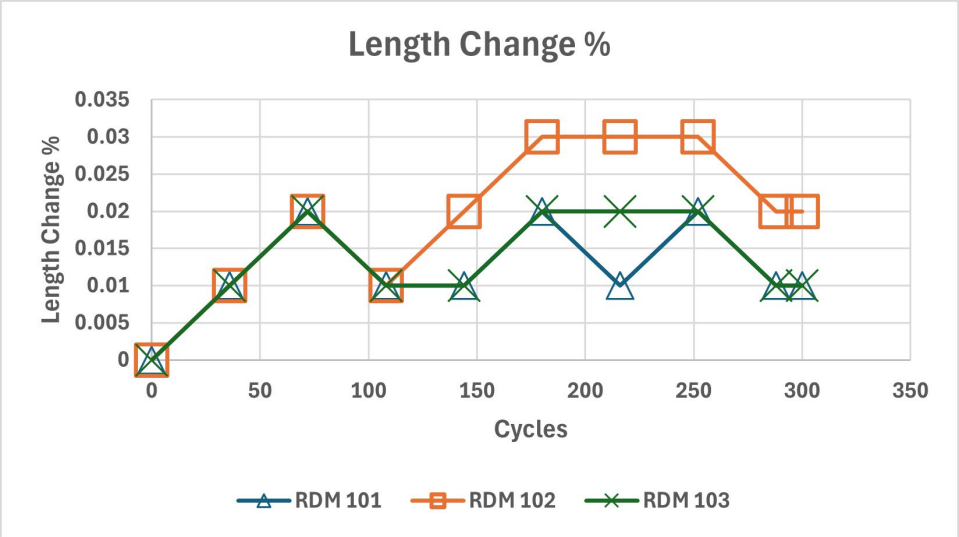

Figure 4.10 Length Change

4.5 Chapter Summary

The data does not show any concern with paving with the material used. Before showing reduced strength, the peak tensile strength was much higher than typical standards. However, it will be prudent to ascertain if the strength loss continues ad-infinitum or if and when it begins to build up again. Compressive strength values were higher than those of control Cell 2405 that was constructed in 2024 on the MnROAD mainline pavement. However, cognizance is taken of the very cold temperature at the time of paving this test cell and how those may suppress the early strength gain. Petrographic analysis was requested to provide more explanations for some of these anomalies. Resistivity values were low and thus indicative of a low permeability concrete pavement. The length change values were within normal ranges also.

Chapter 5: Summary of Petrographic Analysis

5.1 Background

The previous chapter presented the initial test results from the test cell. This chapter discusses the results of petrographic analysis and X ray diffraction analysis performed on a core obtained from the test section. Data and results discussed in this chapter are from chemical analysis and petrographic analysis ((6) & (7) conducted by American Engineering Testing who were contractually retained to do so.

In order to ascertain certain characteristics and validate previous observations, a core was taken from the test cell and sent to a local testing lab. The research requested, apart from full petros, an estimate of the current compressive and tensile strength of the sample to ascertain if there was freeze-thaw damage. X-ray diffraction (XRD) and X-ray fluorescence (XRF) analyses were also requested in order to ascertain degree of hydration in the matrix. The research investigators also requested petrographic analysis to ascertain if the high early strength, that is characteristic of the material resulted in interior microcracking. On March 27, 2025, the core was taken from the MnROAD test cell 2437 (Figure 5.1) and sent to a local testing company for the aforementioned petrographic and chemical analyses.

This chapter presents the results of laboratory work performed by the testing firm on one concrete core sample labeled 243725CC01 submitted by the authors on April 9, 2025. A concrete core was obtained from the above-referenced MnROAD cell that was put in place in November 2024, which contained a highly accelerated strength-gaining material. The focus of the analysis was to determine the degree of hydration of the cement phases, to document the presence of any internal microcracking (and associated autogenous re-healing), and to ascertain whether the concrete was damaged by early-age freezing. The scope of work was limited to performing petrographic and X-ray diffraction analysis on the sample to document the aforementioned concrete properties and quantify the residual cement phases in the binder.

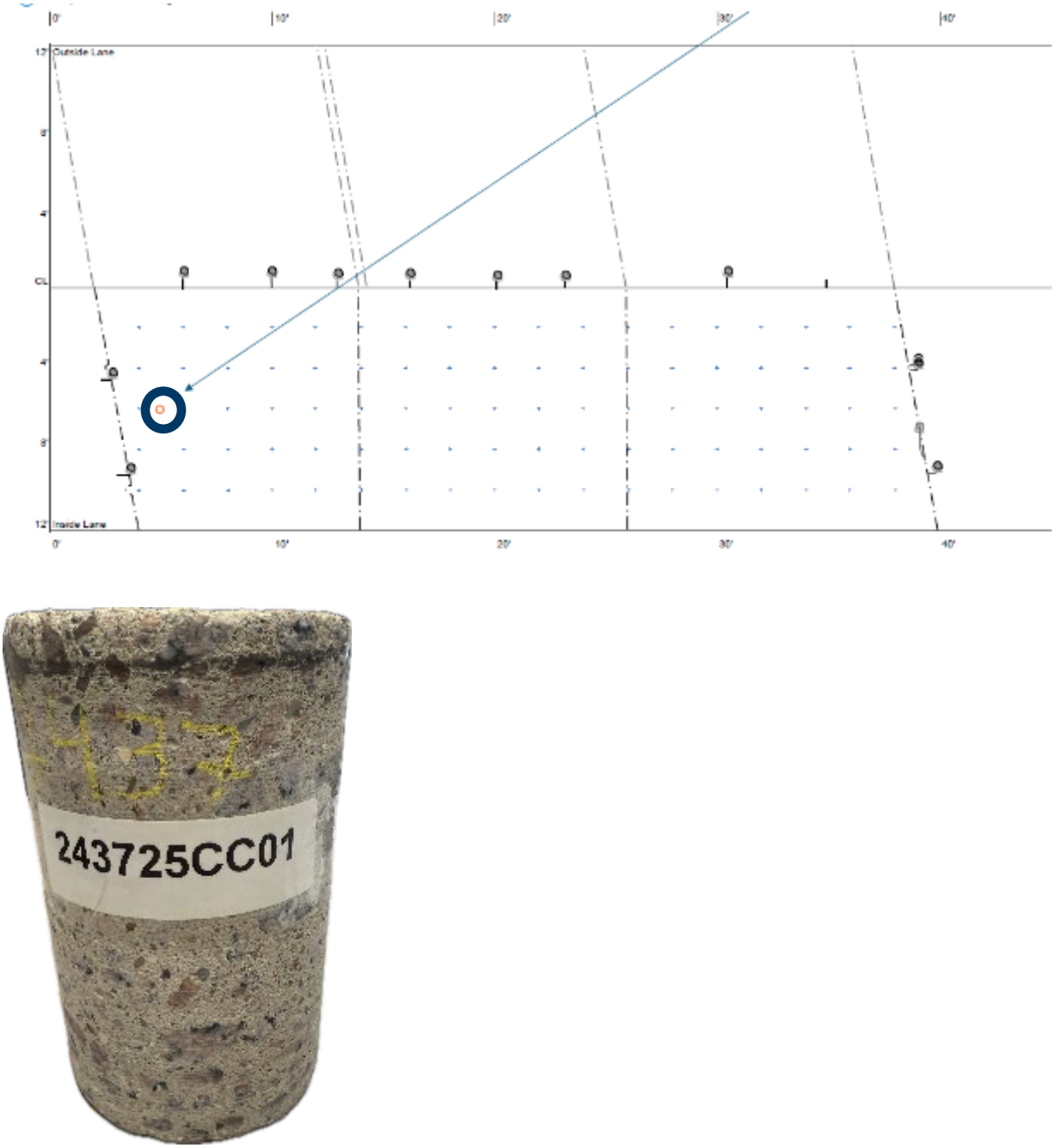

Figure 5.1: (above) Core location sketch, (below) extracted core

Figure 5.1 shows the location at which the 4-inch diameter core was taken. Note that Cell 37 had skewed joints but when cell 2437 was placed, non-skewed joints were established by sawing.

5.2 Test Procedures

Laboratory testing was performed on April 10, 2025, and subsequent dates included petrographic analysis and X-ray diffraction analysis.

5.2.1 Petrographic Analysis

A petrographic analysis was performed in accordance with Standard Operating Procedure 24- LAB-001, "Petrographic Examination of Hardened Concrete," ASTM C856-latest revision. The petrographic analysis consisted of reviewing the cement paste and aggregate qualities on saw cut, lapped, and fractured sections. Reflected light microscopy was performed under an Olympus SZX-12 binocular stereozoom microscope at magnifications up to 160x. The depth of carbonation was documented using a phenolphthalein pH indicator solution applied on freshly saw cut and lapped surfaces of the concrete sample. The paste-coarse aggregate bond quality was determined by fracturing a sound section of the concrete in the laboratory with a rock hammer.

The water/cementitious content of the concrete was estimated by viewing a thin section under a Nikon E600 polarizing light microscope at magnifications of up to 600x. Thin section analysis was performed in accordance with Standard Operating Procedure 24-LAB-009, "Determining the Water/Cement of Portland Cement Concrete, AET Method." An additional, smaller, saw cut subdivision of the concrete sample was epoxy impregnated, highly polished, and then attached to a glass slide using an optically clear epoxy. Excess sample was saw cut from the glass and the thin slice remaining on the slide was lapped and polished until the concrete reached 25 microns or less in thickness. Thin section analysis allows for the observation of Portland cement morphology, including phase identification, an estimate of the amount of residual material, and spatial relationships. Also, the presence and relative amounts of supplementary cementitious materials and pozzolans may be identified and estimated.

5.2.2 X-ray Diffraction Analysis

X-ray diffraction was performed on a Bruker D2 Phaser equipped with a Copper tube radiation source with a slit opening of 1 mm. Measurements were made with an operating voltage of 30 kV and amperage of 10 mA. Diffraction counts were gathered with a Lynxeye detector at an angle of 5 degrees. Binder material was extracted from the sample by drill press and was screened over a #200 sieve; passing material was then scanned from approximately 5 degrees to 65 degrees 2 theta. The data collected was compared to the PDF-4 International Center for Diffraction Data database for phase identification and was processed with Profex® Rietveld Refinement software for phase quantification.

Table 5.1 Measured Relative Abundance of Concrete Component

Phase	Relative %Abundance
Quartz	50.6
Plagioclase Feldspar	12.3
K-Feldspar	8.7
Calcite	2.6
Dolomite	3.1
Inconclusive	0.7
Belite	7.8
Portlandite	0.2
Ettringite	14.0

Table 5.1 shows the result of relative abundance based on XRD analysis. Both the PDF-4 Minerals database and Profex structure files both contain all the known phases of both portland and B-CSA cement, that the petrographers have used to identify and quantify ye'elimite /Klein's compound in CSA products in the past. XRD analysis of the raw cement product would have been much more beneficial in determining the presence of any characteristic product, as drilled material from hardened concrete contains significantly more interferences. XRD analysis gives crystalline content and may not detect amorphous aluminum hydroxide (AH3) and calcium aluminosilicate hydrate (C-A-S-H) which is the primary binding gel, similar to calcium silicate hydrate (C-S-H) but with aluminum (A) incorporated. C-A-S-H is encountered in blended cements as well as some calcium sulfoaluminate cements.

5.3 Investigation of Microcracks

Self-healing phenomena in cementitious materials (e.g. historic Roman concrete/masonry) are eventuated by the presence of coarse lime (CaO) nodules within the binder. The lime nodules react with moisture to form portlandite ($Ca(OH)_2$). Once cracks have begun to form this deposit forms calcite ($CaCO_3$). Calcite was not observed within the autogenous drying-shrinkage microcracks in the analyzed sample. Instead, it appears that ettringite formed preferentially within them.

5.4 General Physical Aggregate and Cementitious Content Observation

Coarse aggregates were 19 mm (3/4") nominal-sized, quarried and crushed granite with a few basalt particles. The particles were mostly sub-angular in shape. The coarse aggregate appeared well graded

and exhibited good overall distribution. Fine aggregates were found to be natural quartz, feldspar, and lithic sand (carbonates, basalt, felsite, greywacke, granite, gabbro, and siltstone with a few iron oxide, shale, and amphibole particles). The grains were mostly sub-rounded with many smaller sub-angular particles. The fine aggregate appeared fairly graded and exhibited good overall uniform distribution.

Although the derived air content was not determined, depth of carbonation was negligible and paste aggregate bond was classified as good, and shrinkage cracks were commonly filled with ettringite. The water/cementitious ratio was estimated at between 0.33 and 0.38 with approximately 8 to 10% residual Portland cement clinker particles.

5.5 Selected Petrographic Images

Figures 5.2 to 5.10 shows pictures of the selected petrographic images.

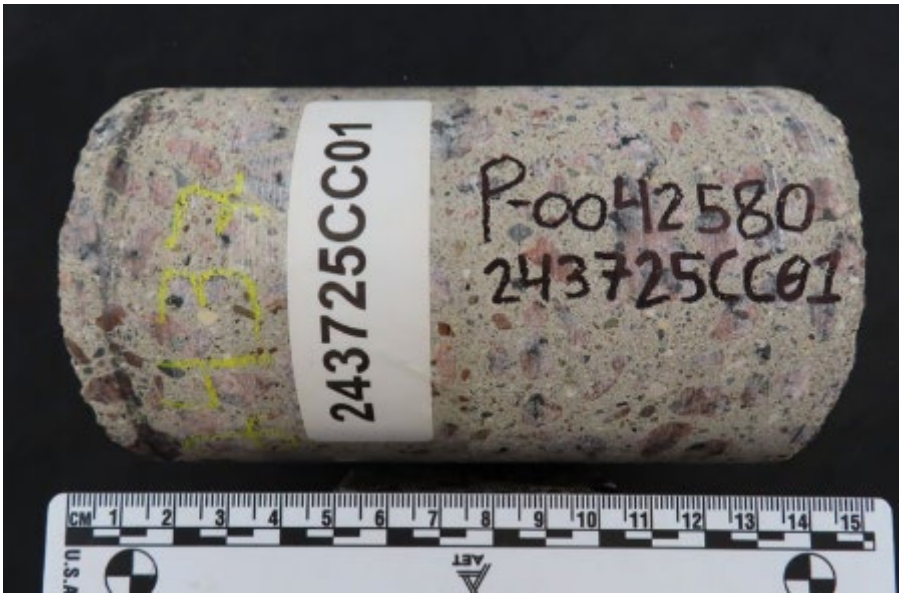

Figure 5.2 MnROAD Core sample 243725CC01 Description: Profile of the core sample as received with the top surface to the left.

Figure 5.3 The drag textured top surface bearing AMS curing compound as received. MnROAD Core sample 243725CC01 Description: Profile of the core sample as received with the top surface to the left.

Figure 5.4: Saw cut and lapped cross section with the top surface oriented to the top of the photo.

There was no detectable segregation shown in Figure 5.4. Microcracks, visible at low magnification, were mapped in red ink, and phenolphthalein pH indicator was applied to top right corner.

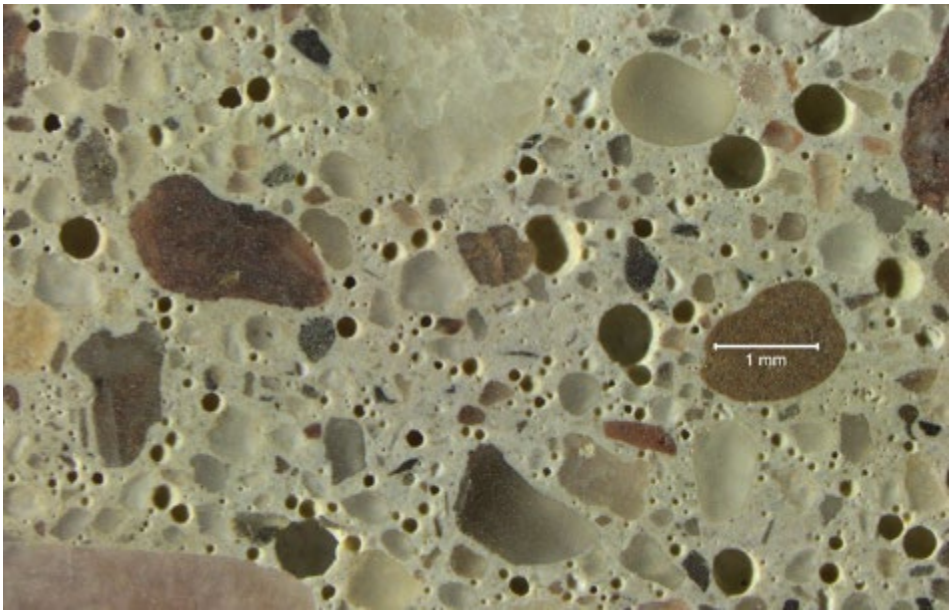

Figure 5.5 Hardened air-void system at depth in the sample on a saw cut 16x and lapped cross section at magnification.

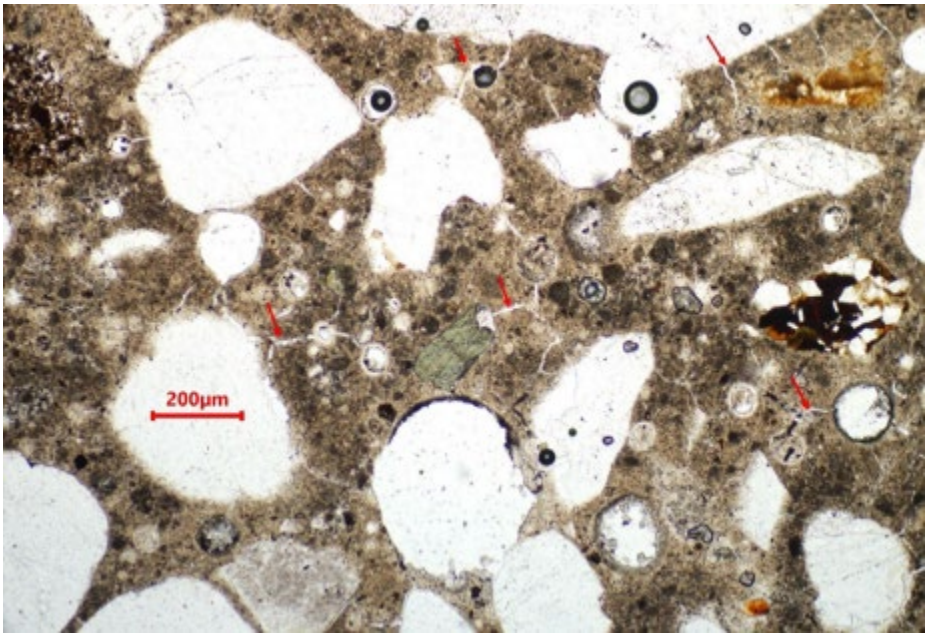

Figure 5.6 Ubiquitous autogenous drying-shrinkage microcracking throughout the concrete paste, as viewed in thin section with transmitted plane polarized light

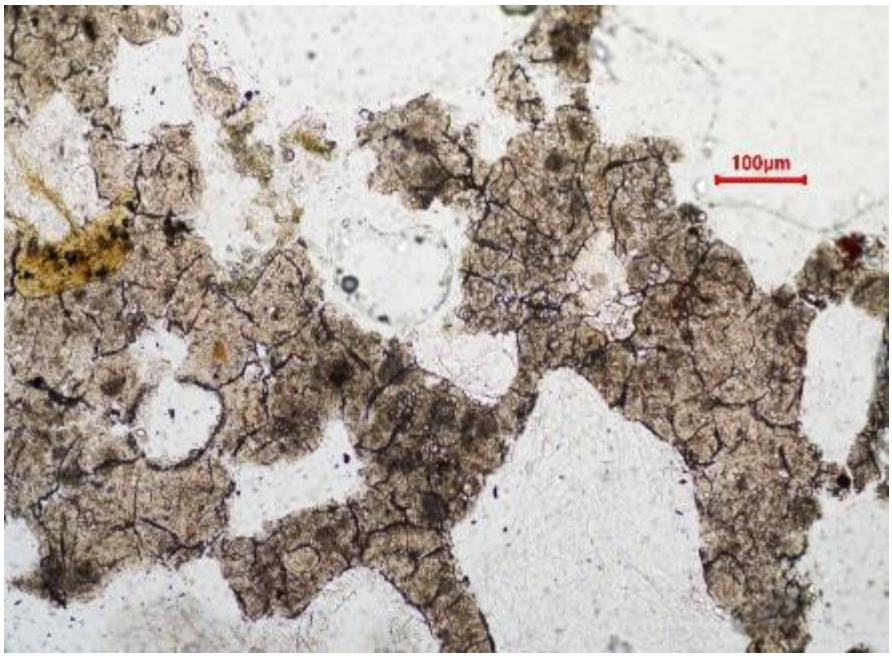

Figure 5.7: Alternate view of the ubiquitous autogenous drying-shrinkage microcracking throughout the concrete paste, as viewed in thin section with transmitted plane polarized light.

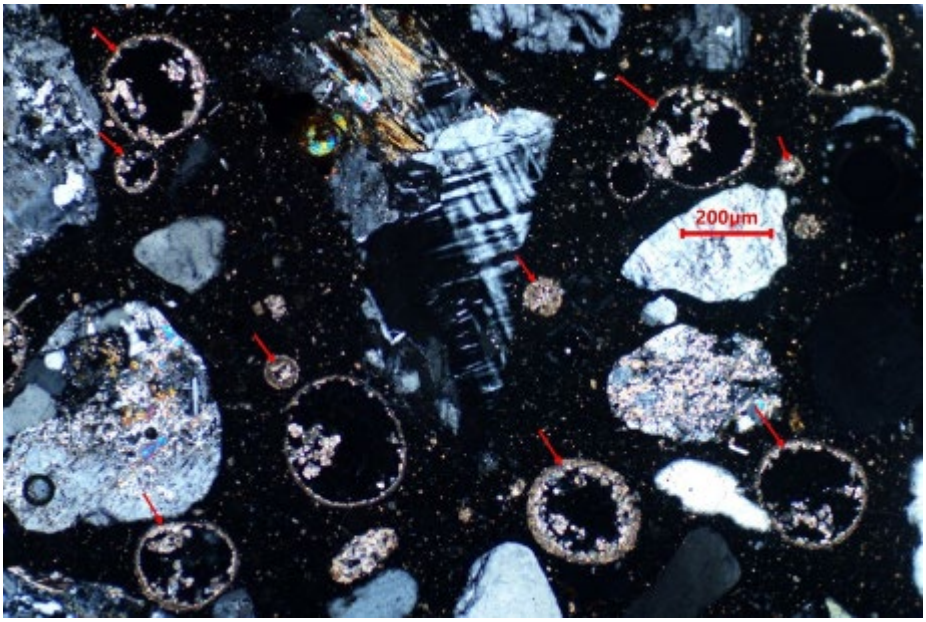

Figure 5.8 Brightly colored secondary calcite that lined to filled most visible air voids in thin 100x section, as viewed with transmitted cross polarized light.

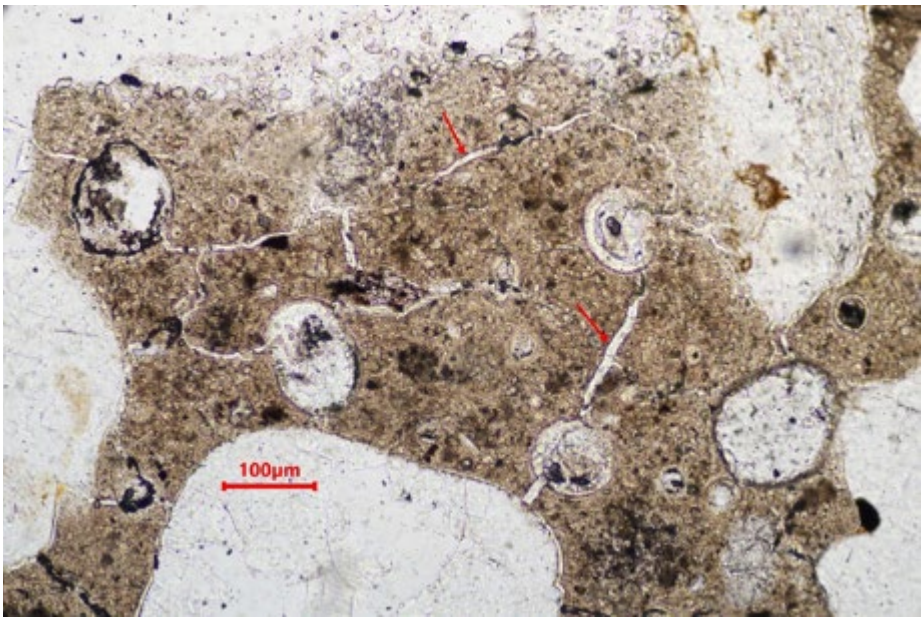

Figure 5.9 Autogenous drying-shrinkage microcracking within the concrete paste, as viewed in thin section with transmitted plane polarized light.

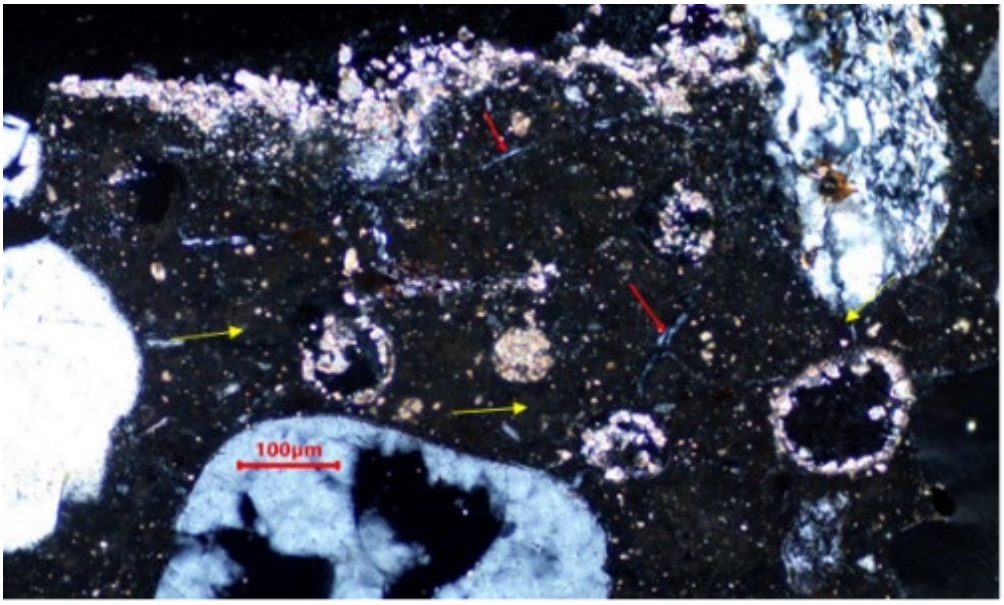

Figure 5.10 Same view as above in transmitted cross polarized light. Many of the autogenous shrinkage cracks were filled by a secondary deposit, likely ettringite. Note secondary carbonate lining to partially filling air voids (yellow arrows).

5.6 Chapter Summary

The concrete was well consolidated and was placed at a low water-to-cement ratio, estimated at between 0.33 and 0.38. Thin section analysis of the concrete sample revealed ubiquitous autogenous drying-shrinkage microcracking throughout the cement paste. The autogenous microcracks were visually consistent with those found in very low water-to-cement ratio (w/cm) mixes, which are driven by elevated water demand from the increased cement concentration. The microcracking was very fine and commonly filled with a secondary deposit optically consistent with ettringite. Due to the relatively high ettringite content, detected by X-ray diffraction analysis of a sample of the binder the secondary deposit was assumed to be ettringite. The microcracking was not able to be visually resolved on the lapped cross section of the core sample under a stereozoom microscope with reflected light at magnification up to 100x. Most air voids observed in thin section were lined and filled with secondary calcite. Several fine air voids, approximately 25 µm in diameter, were lined by ettringite. Frost crystals typically form prior to the cementitious material reaching a compressive strength of approximately 500 psi. No frost crystal impressions were observed on or near the top surface of the analyzed sample. Visually, the concrete comprised a mixture of quarried and crushed igneous rock, coarse aggregate, natural sand fine aggregate. The core sample appeared purposefully air entrained with a well distributed air void system.

Chapter 6: Conclusion and Recommendations

The project investigated the field characteristic of concrete made of an rapid-strength Belitic Calcium Sulfoaluminate concrete placed in Cell 2437 MnROAD. Accelerating early strength gain without loss of durability is an important property desirable in concrete. Consequently, the concrete placed in cell 2437 on the November 22, 2024, using a roller screed was shown to be an acceptable material that gained strength rapidly , withstood frost and passed the ASTM C666 durability test.

In test cell 2437, the initial observations of anomalous initial lowering of flexural strength in comparison to the control after an initially high early peak had necessitated petrographic and chemical analysis of a core. Otherwise, the compressive strength was high and transport properties that were studied over time indicated a fairly impermeable concrete.

Conditions in the field as seen from the thermistors and maturity data showed that the pavement froze after 6 days and went through cycles of freezing and unfreezing for the remaining period before the completion of the 56-day maturity monitoring period. Nevertheless, strength prediction equations were still developed with the maturity data based on early compressive and flexural strength. More importantly petrographic analysis showed no evidence of freezing damage to the material in spite of the cold temperature exposure.

Additionally, the core taken from the pavement, 4 months after paving, passed the ASTM C666 test for freeze thaw durability. Petrographic analysis revealed micro-cracking dispersed within the matrix and filled with ettringite. Material was found to be constructible in spite of the anomalous thixotropic tendency it exhibited in transforming from a very mobile and workable mix quickly to a stiff mix within the period of placement and finishing. Petrographic analysis showed no freeze-thaw damage but revealed evidence of microcracks that were filled with ettringite. When petrographic analyses were repeated by the testing company, results showed a very low presence of Alite, which is chemically unanticipated of BCSA but could be a resemblance of other components, including unreacted Ye'elemite or the aggregate in the matrix. Identification of that component was thus inconclusive from the 2 iterations of petrographic and X-ray diffraction tests performed.

References

1) Neville, A.M. (2011) *Properties of Concrete*. 5th ed. Harlow: Pearson Education.

2) Kienzle A, Thomas RJ. Engineering properties and setting time of belitic calcium sulfoaluminate (BCSA) cement concrete. *Construction and Building Materials.* 2022 Oct 17;352:128979.

3) Živica V. (2000) Properties of blended sulfoaluminate belite cement. *Construction and building Materials*. 2000 Dec 1; 14(8):433-7.

4) Rohne, R.J. and Izevbekhai, B.I. (2009) *Demonstration of Concrete Maturity Test Process on TH-694/TH-35E Interchange–Unweave the Weave* (No. MN/RC 2009-26). Minnesota. Dept. of Transportation.

5) Podolsky J, Velasquez R, Bautista E, Izevbekhai B. (2024) Feasibility of Pavement Temperature as a Surrogate for Performance of Rigid Pavements. In *Proceedings of the International Conference on Concrete Pavements* 2024 Aug 29 (pp. 484-498).

6) Minnesota Dept of Transportation. (2025) American Engineering Testing Report of Petrographic Analysis AET Project No.: P-0042580 Project: MnROAD Cell 2437 Minnesota Dept of Transportation. Revised Report After Second Petro and XRD Testing, submitted to Authors 10/30/2025 (MnDOT OMRR Internal Document)

7) Minnesota Dept of Transportation. (2025) American Engineering Testing Report of Petrographic Analysis AET Project No.: P-0042580 Project: MnROAD Cell 2437 Report of Petro and XRD Testing, Submitted to Authors 05/19/2025 (MnDOT OMRR Internal Document)